

Imaginary spin-orbital coupling in parity-time symmetric systems with momentum-dependent gain and loss

Jieli Qin¹, Lu Zhou^{2,4}, Guangjiong Dong^{3,4}

¹ School of Physics and Materials Science, Guangzhou University, 230 Wai Huan Xi Road, Guangzhou Higher Education Mega Center, Guangzhou 510006, China

² Department of Physics, School of Physics and Electronic Science, East China Normal University, Shanghai 200241, China

³ State Key Laboratory of Precision Spectroscopy, East China Normal University, Shanghai 200241, China

⁴ Collaborative Innovation Center of Extreme Optics, Shanxi University, Taiyuan, Shanxi 030006, China

E-mail: 104531@gzhu.edu.cn, lzhou@phy.ecnu.edu.cn, gjdong@phy.ecnu.edu.cn

December 2021

Abstract. Spin-orbital coupling (SOC) and parity-time (\mathcal{PT}) symmetry both have attracted paramount research interest in condensed matter physics, cold atom physics, optics and acoustics to develop spintronics, quantum computation, precise sensors and novel functionalities. Natural SOC is an intrinsic relativistic effect. However, there is an increasing interest in synthesized SOC nowadays. Here, we show that in a \mathcal{PT} -symmetric spin-1/2 system, the momentum-dependent balanced gain and loss can synthesize a new type of SOC, which we call imaginary SOC. The imaginary SOC can substantially change the energy spectrum of the system. Firstly, we show that it can generate a pure real energy spectrum with a double-valleys structure. Therefore, it has the ability to generate supersolid stripe states. Especially, the imaginary SOC stripe state can have a high contrast of one. Moreover, the imaginary SOC can also generate a spectrum with tunable complex energy band, in which the waves are either amplifying or decaying. Thus, the imaginary SOC would also find applications in the engineering of \mathcal{PT} -symmetry-based coherent wave amplifiers/absorbers. Potential experimental realizations of imaginary SOC are proposed in cold atomic gases and systems of coupled waveguides constituted of nonlocal gain and loss.

Keywords: spin-orbit coupling, parity-time symmetry, cold atoms, coupled waveguides

Submitted to: *New J. Phys.*

1. Introduction

Spin-orbit coupling (SOC) arises from the relativistic-induced coupling between a particle's spin degree of freedom and its momentum. It plays a significant role in

various physical systems. For relativistic elementary particles, SOC leads to their Zitterbewegung oscillation [1]. For atoms, SOC gives rise to the fine structure spectra [2]. And in condensed matter physics, the investigation of SOC has led to fruitful achievements (such as the spin-Hall effect [3], topological insulator [4], just name a few) with potential applications in spintronics [5] and quantum computations [6]. Currently, SOC researches are drastically expanding to the fields of cold atom physics [7–22], optics [23–29] and acoustics [30–34]. Cold atom systems have no natural SOC, whereas using the Raman coupling scheme [11] (and also some others, see the review article [12]) artificial SOC has been experimentally realized, furthermore supersolid stripe states [13–20] and momentum-space Josephson oscillations [21, 22] can be generated. In photonics, the subwavelength scales and additional degrees of freedom of structured optical field are explored, and in such fields, spin and orbital properties are strongly coupled with each other [23]. In a birefringent optical fiber, traveling of the light pulses with mutually orthogonal linear polarizations is described by a set of nonlinear Schrödinger equations with a SOC Hamiltonian [24, 25]. In dual-core waveguides, SOC can be synthesized by dispersively coupling the light field in different cores [26–28], and stripe solitons can be produced [29]. In acoustical systems, SOC has also been successfully synthesized [30–34].

Non-Hermitian parity-time (\mathcal{PT}) symmetry physics is another active researching field these days [35–38]. The seminal work by Bender and Boettcher in 1998 states that a non-Hermitian Hamiltonian with \mathcal{PT} -symmetry can support complete real value eigenenergies [39], and this has boosted the investigation of non-Hermitian quantum mechanics [40–45]. Considering the analogy of classical wave equation to the quantum mechanics Schrödinger equation, \mathcal{PT} -symmetric Hamiltonian can be used to model the balanced gain and loss, and has been realized in systems of optics [46, 47], acoustics [48–51], and many others [52–58]. Fruitful applications such as invisible acoustic sensors [59], microcavity sensors [60, 61], unidirectional transportation [62–64], light-light switch [65], and laser amplifier/absorber [66–71] were born out.

Recently, researches on momentum-dependent gain and loss are emerging. In cold atomic gas systems, the gain can be realized by injecting atoms into the condensate using an atom laser [72], while the loss can be realized by exciting atoms firstly to an excited state with a laser beam and then ejecting them out from the condensate via photon recoil [73]. Due to the momentum-distribution of the atom laser [74, 75], and the Doppler effect in atom-light interaction [76], gain and loss realized in these ways have a distinct momentum-dependence. In the optical medium, spatially nonlocal gain and loss after a Fourier transformation are wavevector-dependent (or equivalently “momentum”-dependent) [77, 78], and this feature has been proposed to explore the topological physics in photonic systems [79].

Here, we show that in \mathcal{PT} -symmetric spin-1/2 systems, momentum-dependent gain and loss can synthesize an imaginary interaction between the spin degree of freedom and the orbital motion, thus an imaginary SOC (for comparison, the conventional SOC will be termed as “real SOC” in the following). Next, we present the imaginary

SOC Hamiltonian, and study its properties at first, leaving the discussion on potential experimental realizations in cold atom physics and optical systems to the end of the paper.

2. Model

We study a spin-1/2 Hamiltonian in momentum representation given by

$$H = \frac{|\vec{p}|^2}{2m} \sigma_0 + i\hbar\gamma\Theta(\vec{p})\sigma_z + \hbar\Omega\sigma_x, \quad (1)$$

where σ_0 , $\sigma_{x,y,z}$ are the conventional 2×2 unitary and Pauli matrices, m is the particle mass, \vec{p} is the momentum operator, \hbar is the Planck constant, γ represents the rate of the balanced gain and loss, $\Theta(\vec{p})$ is a positive dimensionless function with its maximum normalized to 1 [i.e., $0 \leq \Theta(\vec{p}) \leq 1$], and it is used to describe the profile of momentum-dependence of the balanced gain and loss, at last Ω is the Rabi coupling strength between the two spin components.

If $\Theta(\vec{p})$ is imaginary, the second term in Hamiltonian (1) is real, and represents an interaction between the spin and a momentum-dependent magnetic field along the z -direction. Thus, it is a conventional real SOC term. For example, when $\Theta(\vec{p}) = ip_x$, the Hamiltonian (1) has the same form as that in the SOC cold atom system realized with the Raman coupling scheme [11]. However, in the present paper, $\Theta(\vec{p})$ is a profile function describing the momentum-dependence of the gain and loss, that is to say it is a real function, hence the second term of the Hamiltonian is imaginary, thus termed as “imaginary SOC”. This imaginary SOC Hamiltonian is \mathcal{PT} -symmetric, with the parity operator \mathcal{P} exchanging the two spin components, and the operator \mathcal{T} performing the complex conjugation [35]. We also note that there already exist some researches combining SOC and \mathcal{PT} symmetry [80–84], however in these works it is a conventional Hermitian SOC term and a \mathcal{PT} -symmetric term been stiffly glued. In contrast, here the SOC term itself is non-Hermitian.

To analytically understand the properties of imaginary SOC, we solve the eigenvalue problem of Hamiltonian (1). The eigenenergies and corresponding eigenvectors are

$$E_{\pm} = \frac{|\vec{p}|^2}{2m} \pm \hbar\sqrt{\Omega^2 - \gamma^2\Theta^2(\vec{p})}, \quad (2)$$

and

$$\psi_{\pm} = \frac{1}{A} \begin{bmatrix} \left(i\gamma\Theta(\vec{p}) \pm \sqrt{\Omega^2 - \gamma^2\Theta^2(\vec{p})} \right) / \Omega \\ 1 \end{bmatrix}, \quad (3)$$

with A_{\pm} being normalization constants. When $\Omega \geq \gamma$, the eigenenergies E_{\pm} always take real values, and the eigenvectors can be simplified to $\psi_{\pm} = [\pm \exp(\pm i\theta), 1]^T / \sqrt{2}$ with $\theta = \arcsin[\gamma\Theta(\vec{p})/\Omega]$, and “T” denoting the transpose operation. It is seen that these eigenvectors are \mathcal{PT} -symmetric with equal spin amplitudes $|\psi_{\pm,\uparrow}| = |\psi_{\pm,\downarrow}|$. Considering the dynamical factor $\exp[-iE_{\pm}t/\hbar]$, the states will evolve with their norms conserved due to the exact balance between loss and gain. When $\Omega < \gamma$, the states with

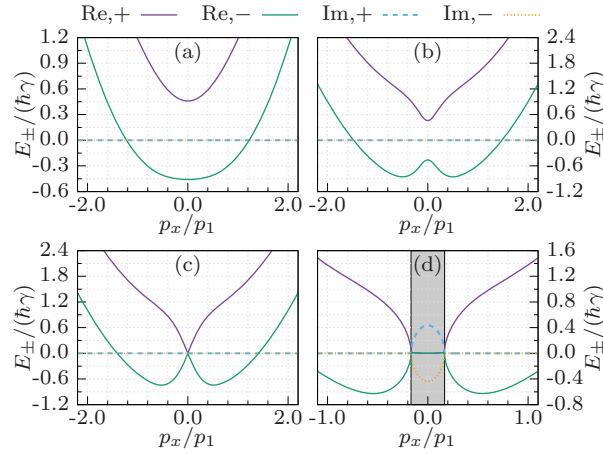


Figure 1. Energy spectra $E_{\pm}(p_x)$ for imaginary SOC with momentum-dependence profile $\Theta(p_x)$ given by Eq. (4). The real (Re) parts of E_+ and E_- are plotted as the solid violet and green lines, while their imaginary (Im) parts are plotted as the cyan dashed and brown dotted lines. Panels (a,b): Pure real spectra for $\Omega = 1.1\gamma > \gamma$. Under these parameters, the critical gain/loss momentum-space width separates the single- and double-valleys spectrum is $\sigma_c = 2.09p_1$ with $p_1 = \sqrt{m\hbar\gamma}$. Panel (a): Single-valley energy spectrum for $\sigma = 2.5p_1 > \sigma_c$. Panel (b): Double-valleys energy spectrum for $\sigma = 0.5p_1 < \sigma_c$. Panel (c): Pure real gapless energy spectrum for $\Omega = \gamma$ and $\sigma = 0.5p_1$. Panel (d): Complex energy spectrum for $\Omega = 0.9\gamma < \gamma$ and $\sigma = 0.5p_1$. In the gray color filled band, the spectrum has complex eigenenergy.

momentum fulfilling $\gamma^2\Theta^2(\vec{p}) \leq \Omega^2$ are also \mathcal{PT} -symmetric with pure real eigenenergies. However, the states with momentum fulfilling $\gamma^2\Theta^2(\vec{p}) > \Omega^2$ have complex eigenenergies $E_{\pm} = E_R \pm iE_I$ with $E_R = |\vec{p}|^2 / (2m)$ and $E_I = \hbar\sqrt{\gamma^2\Theta^2(\vec{p}) - \Omega^2}$. Now, the dynamical factor becomes $\exp[-iE_{\pm}t/\hbar] = \exp[-iE_Rt/\hbar] \cdot \exp[\pm E_I t/\hbar]$, for $\exp[-E_I t/\hbar]$ the states will automatically decay, while for $\exp[+E_I t/\hbar]$ the states will automatically be amplified during the evolution. The decay and amplify can be understood by examining the corresponding eigenvectors. In this case, the eigenvectors are simplified to $\psi_{\pm} = [i \exp(\pm\vartheta), 1]^T / \sqrt{A_{\pm}}$ with $\vartheta = \text{arccosh}[\gamma\Theta(\vec{p})/\Omega]$ and $A_{\pm} = \sqrt{1 + \exp(\pm 2\vartheta)}$, which have unequal spin amplitudes $|\psi_{\pm,\uparrow}| \neq |\psi_{\pm,\downarrow}|$. Thus, the \mathcal{PT} -symmetry is broken, the gain and loss no longer can cancel each other.

Next, we examine the effect of imaginary SOC on the shape of energy spectrum curve. For facilitation, we particularly consider the one-dimensional case ($\vec{p} = p_x \hat{x}$), and assume that the momentum-dependence profile function $\Theta(p_x)$ takes the Lorentzian shape

$$\Theta(p_x) = \frac{\sigma^2}{p_x^2 + \sigma^2}, \quad (4)$$

where σ is the momentum-space width of the balanced gain and loss.

Firstly, we found that the imaginary SOC can generate spectra with both single-valley and double-valleys structures when $\Omega \geq \gamma$, as shown in panels (a,b) of Fig. 1. The minima and maxima of the spectrum can be found by letting the derivatives of

$E_{\pm}(p_x)$ equal to zero, $dE_{\pm}/dp_x = 0$. The upper branch E_+ of the spectrum always has only one minimum at $p_x = 0$. However, the lower branch E_- can have either one or two minima, depending on the value of σ . When σ is larger than the critical value $\sigma_c = \sqrt{2m\hbar}\gamma/(\Omega^2 - \gamma^2)^{1/4}$, the lower branch also has only one minimum at $p_x = 0$. While for $\sigma < \sigma_c$, the point $p_x = 0$ becomes a maximum, and the lower branch spectrum exhibits a double-valleys structure with two minima located at $p_x = \pm p_0$, which are the solutions of equation $dE_-/dp_x = 0$.

Usually, there is an energy gap between the upper and lower spectrum branches, $\Delta E = 2\hbar\sqrt{\Omega^2 - \gamma^2}$. However, due to the energy band attraction effect in non-Hermitian systems [85, 86], as the strength of the balanced gain and loss increases, the gap becomes narrow, and when $\gamma = \Omega$, it disappears, see panel (c) of Fig. 1. Interesting, even the spectrum becomes gapless, the two spin components are still coupled with each other [see eigenstates (3)], in sharp contrast with the real SOC case where the gapless system is trivial due to the decoupling of the two spin components [11, 15, 87–90].

We also found that the imaginary SOC can generate spectrum with a complex energy band when $\Omega < \gamma$, as shown by the gray color filled rectangle in panel (d) of Fig. 1. In this case, there exist a critical momentum $p_c = \sigma\sqrt{\gamma/\Omega - 1}$ [the solution of $\Omega^2 - \gamma^2\Theta^2(p_x) = 0$], the state with momentum $|p_x| \geq p_c$ still has pure real eigenenergy. However, the eigenenergy corresponding to state with momentum $|p_x| < p_c$ becomes complex, thus forming the complex energy band in the figure. And according to formula $p_c = \sigma\sqrt{\gamma/\Omega - 1}$, this complex energy band can be conveniently tuned by both the gain/loss or Rabi coupling strength.

The above discussion indicates that imaginary SOC would find applications in the fields of energy spectrum engineering and coherent wave amplifying/absorbing. Similar to real SOC, imaginary SOC also can generate spectra with single-valley or double valleys structures. Additionally, imaginary SOC also generates non-trivial gapless spectrum and spectrum with complex energy band, which are absent in the case of real SOC. It has been proposed and experimentally demonstrated that the complex energy modes of a \mathcal{PT} -symmetric optical system can be applied to realize laser amplifiers and absorbers [66–71]. Here we show that imaginary SOC can control the complex energy spectrum, thus provides it the ability to manage \mathcal{PT} -symmetry-based laser amplifiers/absorbers.

3. Imaginary SOC in Harmonic Trap

For the single-valley spectrum, it is easy to imagine that the ground state of a imaginary SOC system will fall into the bottom of this valley. However, for the double-valleys spectrum, the ground state may fall in either the p_0 valley or the opposite $-p_0$ valley. Thus, when an external trapping potential is included, the superposition of these two momentum states can be induced to produce a supersolid stripe state. In this vein of thought, now we consider a case that the imaginary SOC particles are trapped in a harmonic potential $V(x) = \frac{1}{2}m\omega^2x^2$, or equivalently $V(p_x) =$

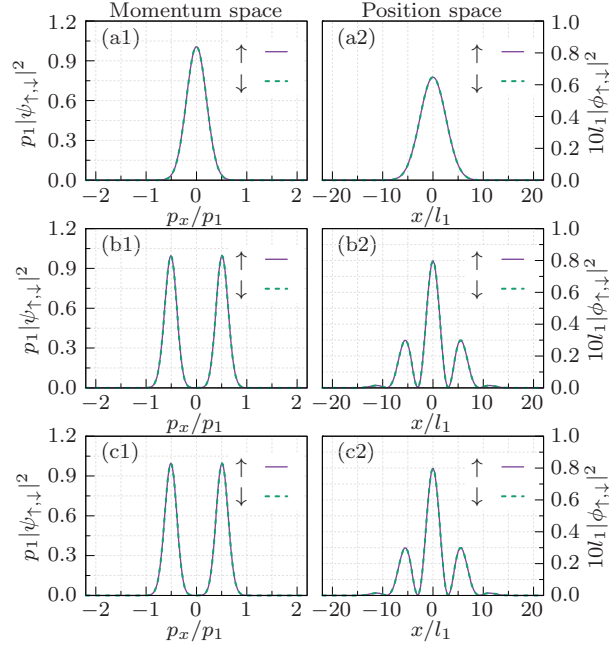


Figure 2. \mathcal{PT} -symmetric normal and supersolid stripe eigenstates generated by imaginary SOC in a harmonic trap. The left panels (a1-c1) show the probability density in momentum space, while the right panels (a2-c2) show the probability density in position space. The spin- \uparrow and spin- \downarrow components are plotted using violet solid and green dashed line respectively (since the states are \mathcal{PT} -symmetric with $|\psi_{\uparrow}| = |\psi_{\downarrow}|$, the two lines overlap with each other). The harmonic trap frequency is $\omega = 0.05\gamma$ for all the panels. Panels (a1, a2): Normal state under parameters $\Omega = 1.1\gamma$, $\sigma = 2.5p_1$ ($p_1 = \sqrt{m\hbar\gamma}$). Panels (b1, b2): Supersolid Stripe state under parameters $\Omega = 1.1\gamma$, $\sigma = 0.5p_1$. Panels (c1, c2): Supersolid Stripe state under parameters $\Omega = \gamma$, $\sigma = 0.5p_1$. The pure real eigenenergies of these states are $E = -0.44\hbar\gamma$ (a), $-0.81\hbar\gamma$ (b), $-0.70\hbar\gamma$ (c). The corresponding free energy spectra are shown in panels (a, b, c) of figure 1.

$-\frac{1}{2}m\hbar^2\omega^2\partial_{p_x}^2$ in the momentum representation. We first numerically diagonalize the full Hamiltonian in the momentum representation to obtain the eigenwavefunctions $\psi_n(p_x) = [\psi_{\uparrow,n}(p_x), \psi_{\downarrow,n}(p_x)]^T$ with $n = 1, 2, \dots$, and further calculate the wavefunction in position representation by Fourier transform, $\phi_n(x) = \int \psi_n(p_x) e^{ip_x x/\hbar} dx / \sqrt{2\pi}$.

In Fig. 2, we show the probability densities of some different eigenstates in both momentum and position space for a weak harmonic trap with frequency $\omega = 0.05\gamma$. Other parameters are chosen corresponding to the free spectra previously shown in panels (a,b,c) of Fig. 1. Panels (a1,a2) correspond to the single-valley spectrum. We see that in momentum space the probability density is centered at $p_x = 0$, which is just the center of the spectrum valley; and in position space, the density is centered at the bottom of the harmonic trap (since it is similar to the ground state of a normal harmonic oscillator, we call it “normal” state). When the free spectrum has a double-valleys structure, we found the probability density of the bound state exhibits two peaks centered around the bottom of the two valleys; and in position space, the expected supersolid stripe structure is observed (“stripe” state), see panels (b1,b2;

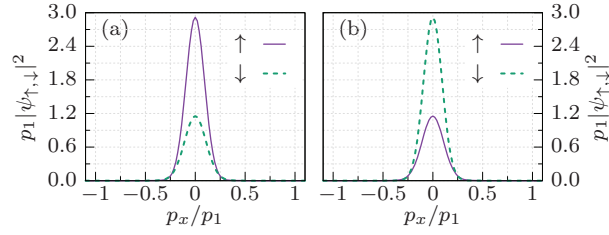


Figure 3. \mathcal{PT} -symmetry broken eigenstates generated by imaginary SOC in a harmonic trap. The probability in momentum space for spin- \uparrow and spin- \downarrow components are plotted as the violet solid and green dashed lines respectively. Panel (a): Decaying eigenstate with complex eigenenergy $E = (0.08 - 0.36i) \hbar \gamma$. Panel (b): Amplifying eigenstate with complex energy $E = (0.08 + 0.36i) \hbar \gamma$. The parameters used are $\omega = 0.05\gamma$, $\Omega = 0.9\gamma$ and $\sigma = 0.5p_1$ ($p_1 = \sqrt{m\hbar\gamma}$). The corresponding free energy spectrum has a complex energy band around $p_x = 0$, as shown in panel (d) of Fig. 1.

c1,c2). Especially, the free spectrum corresponding to panels (c1,c2) is gapless, but the stripe state is also observed. This further demonstrates the non-trivialness of the gapless free spectrum which has been discussed in the previous section. More interesting, we see that the density minimums of the imaginary SOC generated stripe state can drop to zero, i.e., the stripe has a high contrast of one. By comparison, the supersolid stripe realized with the real SOC usually has a poor contrast, leading to difficulty in experimental observation [91–93].

Besides, corresponding to the complex energy band free spectrum [panel (d) of Fig. 1], imaginary SOC can also generate \mathcal{PT} -symmetry broken bounded states in the harmonic trap. The result is shown in Fig. 3. The \mathcal{PT} -symmetry broken states appear in pairs with opposite spin polarization and opposite imaginary parts of eigenenergies, thus one of them is a decaying state, while the other is an amplifying one.

4. Experimental Realizations

Firstly, we propose that imaginary SOC can be realized in cold atom systems. We consider a system of one-dimensional spin-1/2 cold atomic gas with the two spin components coupled by a laser field with Rabi frequency Ω . The momentum-dependent gain in the spin- \uparrow component can be realized by injecting spin- \uparrow atoms into the system using an atom laser with appropriate momentum distribution [72, 74, 75]. Especially, ref. [75] proposed a procedure to produce cold-atom beams with the Lorentzian profile of momentum distribution. And according to ref. [76], exploiting the Doppler shift technique, atoms in the spin- \downarrow state can be velocity-selectively excited to narrow Rydberg or metastable states with a laser, and the following photon recoil could produce a momentum-dependent atomic loss. Denoting the momentum-dependent gain and loss by $\pm i\hbar\gamma\Theta(\vec{p})$, the system can be readily described by the Hamiltonian (1).

Another possible system to realize the imaginary SOC is the coupled planar waveguides with nonlocal gain and loss [77, 78]. We consider a system of two coupled

planar (x - z plane) waveguides, where light propagates along the z -axis, and x is the transverse direction. In the paraxial approximation, the light fields in the two waveguides $E_{\uparrow,\downarrow}$ follow equations [46, 47, 94, 95]

$$i \frac{\partial E_{\uparrow,\downarrow}(z, x)}{\partial z} = - \frac{\lambda_0}{4\pi n_0} \frac{\partial^2 E_{\uparrow,\downarrow}(z, x)}{\partial x^2} + \Omega E_{\downarrow,\uparrow}(z, x) \mp \frac{2\pi}{\lambda_0} \int i\gamma \Xi(x - x') E_{\uparrow,\downarrow}(z, x') dx', \quad (5)$$

where λ_0 is the vacuum wavelength, n_0 is the background refractive index of the waveguides, Ω is the coupling between the two waveguides, and $\pm i\gamma \Xi(x - x')$ describes the nonlocal gain and loss in the two waveguides. Performing Fourier transform on both sides of Eqs. (5), we get

$$i \frac{\partial}{\partial z} \begin{bmatrix} E_{\uparrow}(z, k_x) \\ E_{\downarrow}(z, k_x) \end{bmatrix} = \mathcal{H} \begin{bmatrix} E_{\uparrow}(z, k_x) \\ E_{\downarrow}(z, k_x) \end{bmatrix}, \quad (6)$$

with

$$\mathcal{H} = - \frac{\lambda_0 k_x^2}{4\pi n_0} \sigma_0 + \frac{2\pi}{\lambda_0} i\gamma \Theta(k_x) \sigma_z + \Omega \sigma_x, \quad (7)$$

where $\Theta(\cdot)$ is the Fourier transform of function $\Xi(\cdot)$. Now, it is obvious that Eq. (6) is analogous to an Schrödinger equation in momentum representation, where the “Hamiltonian” \mathcal{H} has the same form as that of Eq. (1), with wavevector k_x playing the role of momentum. Therefore, we propose that the coupled optical waveguides system with nonlocal gain and loss can be used to emulate the imaginary SOC.

5. Summary

In this work, we have proposed a new type of SOC—imaginary SOC, which is induced by momentum-dependent gain and loss, and possesses the property of \mathcal{PT} -symmetry. Imaginary SOC has the ability of energy spectrum engineering. As examples, we firstly show that it can generate pure real energy spectra with double-valleys structures. The interference between waves corresponding to different valleys can produce supersolid stripe states. Compared to the real SOC supersolid stripe state which usually has low contrast, the supersolid stripe state realized by imaginary SOC can have a high contrast of one. What is more, we also shown that the imaginary SOC can generate spectra with tunable band of complex energy, in which the waves are either decaying or amplifying during the time evolution. Thus, the imaginary SOC can also have potential applications in engineering the \mathcal{PT} -symmetry-based coherent wave amplifiers/absorbers. For experimental realization, we propose that the imaginary SOC can be implemented in spin-1/2 cold atomic gases and also in systems of coupled waveguides.

Acknowledgments

J. L. Qin acknowledges the support from National Natural Science Foundation of China (11904063). G. J. Dong acknowledges the financial support from Shanghai

Municipal Education Commission (2019-01-07-00-05-E00079), National Natural Science Foundation of China (11574085, 11834003, 91536218), National Key Research and Development Program of China (2017YFA0304201) and Overseas Expertise Introduction Project for Discipline Innovation (B12024). L. Zhou acknowledges the support from National Natural Science Foundation of China (12074120) and Science and Technology Commission of Shanghai Municipality (Grant No. 20ZR1418500).

Reference

- [1] Schrödinger E 1930 Über die kräftefreie Bewegung in der relativistischen Quantenmechanik, *Sitzungsber. Preuss. Akad. Wiss. Phys. Math. Kl.* **24**, 418
- [2] Bernath P F 2005 *Spectra of atoms and molecules* (Oxford University Press: New York).
- [3] Sinova J, Valenzuela S O, Wunderlich J, Back C H and Jungwirth T 2015 Spin Hall effects *Rev. Mod. Phys.* **87** 1213
- [4] Hasan M Z and Kane C L 2010 Colloquium : Topological insulators *Rev. Mod. Phys.* **82** 3045
- [5] Žutić I, Fabian J and Das Sarma S 2004 Spintronics: fundamentals and applications *Rev. Mod. Phys.* **76**,323 (2004).
- [6] Kloeffer C and Loss D 2013 Prospects for spin-based quantum computing in quantum dots *Annu. Rev. Condens. Matter Phys.* **4** 51
- [7] Zhai H 2012 Spin-orbit coupled quantum gases *Int. J. Mod. Phys. B* **26** 1230001
- [8] Galitski V and Spielman I B 2013 Spin-orbit coupling in quantum gases *Nature* **494** 49
- [9] Zhai H 2015 Degenerate quantum gases with spin-orbit coupling: a review *Reports Prog. Phys.* **78** 026001
- [10] Zhang Y, Mossman M E, Busch T, Engels P and Zhang C 2016 Properties of spin-orbit-coupled Bose-Einstein condensates *Front. Phys.* **11** 118103
- [11] Lin Y-J, Jimenez-Garcia K and Spielman I B 2011 Spin-orbit-coupled Bose-Einstein condensates *Nature* **471** 83
- [12] Zhang S and Jo G B 2019 Recent advances in spin-orbit coupled quantum gases *J. Phys. Chem. Solids* **128** 75
- [13] Li Y, Pitaevskii L P and Stringari S 2012 Quantum tricriticality and phase transitions in spin-orbit coupled Bose-Einstein condensates *Phys. Rev. Lett.* **108** 225301
- [14] Hu H, Ramachandran B, Pu H and Liu X J 2012 Spin-orbit coupled weakly interacting bose-einstein condensates in harmonic traps *Phys. Rev. Lett.* **108** 010402
- [15] Achilleos V, Frantzeskakis D J, Kevrekidis P G and Pelinovsky D E 2013 Matter-wave bright solitons in spin-orbit coupled Bose-Einstein condensates *Phys. Rev. Lett.* **110** 264101
- [16] Li J-R, Lee J, Huang W, Burchesky S, Shteynas B, Top F Ç, Jamison A O and Ketterle W 2017 A stripe phase with supersolid properties in spin-orbit-coupled Bose-Einstein condensates *Nature* **543** 91
- [17] Bersano T M, Hou J, Mossman S, Gokhroo V, Luo X-W, Sun K, Zhang C and Engels P 2019 Experimental realization of a long-lived striped Bose-Einstein condensate induced by momentum-space hopping *Phys. Rev. A* **99** 051602
- [18] Luo X W and Zhang C 2019 Tunable spin-orbit coupling and magnetic superstripe phase in a Bose-Einstein condensate *Phys. Rev. A* **100** 063606
- [19] Putra A, Salces-Cárcoba F, Yue Y, Sugawa S and Spielman I B 2020 Spatial coherence of spin-orbit-coupled Bose gases *Phys. Rev. Lett.* **124** 053605
- [20] Zhao L-C, Luo X-W and Zhang C 2020 Magnetic stripe soliton and localized stripe wave in spin-1 Bose-Einstein condensates *Phys. Rev. A* **101** 023621
- [21] Hou J, Luo X-W, Sun K, Bersano T, Gokhroo V, Mossman S, Engels P and Zhang C 2018 Momentum-space Josephson effects *Phys. Rev. Lett.* **120** 120401

- [22] Zheng Y, Feng S and Yang S-J 2018 Josephson oscillation and self-trapping in momentum space *Phys. Rev. A* **97** 043627
- [23] Bliokh K Y, Rodríguez-Fortuño F J, Nori F and Zayats A V. 2015 Spin-orbit interactions of light *Nat. Photonics* **9** 796
- [24] Menyuk C R 1989 Pulse propagation in an elliptically birefringent Kerr medium *IEEE J. Quantum Electron.* **25** 2674
- [25] Malomed B A 1991 Polarization dynamics and interactions of solitons in a birefringent optical fiber *Phys. Rev. A* **43** 410
- [26] Chiang K S, Chow Y T, Richardson D J, Taverner D, Dong L, Reekie L and Lo K M 1997 Experimental demonstration of intermodal dispersion in a two-core optical fibre *Opt. Commun.* **143** 189
- [27] Kartashov Y V., Konotop V V. and Malomed B A 2015 Dark solitons in dual-core waveguides with dispersive coupling *Opt. Lett.* **40** 4126
- [28] Kartashov Y V., Malomed B A, Konotop V V., Lobanov V E and Torner L 2015 Stabilization of spatiotemporal solitons in Kerr media by dispersive coupling *Opt. Lett.* **40** 1045
- [29] Sakaguchi H and Malomed B A 2016 One- and two-dimensional solitons in PT-symmetric systems emulating spin-orbit coupling *New J. Phys.* **18** 105005
- [30] Ju F, Cheng Y and Liu X 2018 Acoustic spin Hall-like effect in hyperbolic metamaterials controlled by the helical wave *Sci. Rep.* **8** 1
- [31] Bliokh K Y and Nori F 2019 Spin and orbital angular momenta of acoustic beams *Phys. Rev. B* **99** 174310
- [32] Deng W, Huang X, Lu J, Peri V, Li F, Huber S D and Liu Z 2020 Acoustic spin-Chern insulator induced by synthetic spin-orbit coupling with spin conservation breaking *Nat. Commun.* **11** 3327
- [33] Gao M, Wu S and Mei J 2020 Acoustic topological devices based on emulating and multiplexing of pseudospin and valley indices *New J. Phys.* **22** 013016
- [34] Wang S, Zhang G, Wang X, Tong Q, Li J and Ma G 2021 Spin-orbit interactions of transverse sound *Nat. Commun.* **12** 6125
- [35] Bender C M 2007 Making sense of non-Hermitian Hamiltonians *Reports Prog. Phys.* **70** 947
- [36] D. Christodoulides and J. Yang, editors 2018 *Parity-time symmetry and its applications* (Springer: Singapore)
- [37] El-Ganainy R, Makris K G, Khajavikhan M, Musslimani Z H, Rotter S and Christodoulides D N 2018 Non-Hermitian physics and PT symmetry *Nat. Phys.* **14** 11
- [38] Özdemir Ş K, Rotter S, Nori F and Yang L 2019 Parity-time symmetry and exceptional points in photonics *Nat. Mater.* **18** 783
- [39] Bender C M and Boettcher S 1998 Real spectra in non-Hermitian Hamiltonians having PT symmetry *Phys. Rev. Lett.* **80** 5243
- [40] Bender C M, Brody D C and Jones H F 2002 Complex extension of quantum mechanics *Phys. Rev. Lett.* **89** 270401
- [41] Brody D C 2016 Consistency of PT-symmetric quantum mechanics *J. Phys. A Math. Theor.* **49** 10LT03
- [42] Zhang D J, Wang Q H and Gong J 2019 Time-dependent PT-symmetric quantum mechanics in generic non-Hermitian systems *Phys. Rev. A* **100** 062121
- [43] Lee Y C, Hsieh M H, Flammia S T and Lee R K 2014 Local PT symmetry violates the no-signaling principle *Phys. Rev. Lett.* **112** 130404
- [44] Quijandría F, Naether U, Özdemir S K, Nori F and Zueco D 2018 PT-symmetric circuit QED *Phys. Rev. A* **97** 053846
- [45] Wu Y, Liu W, Geng J, Song X, Ye X, Duan C K, Rong X and Du J 2019 Observation of parity-time symmetry breaking in a single-spin system *Science (80-.)*. **364** 878
- [46] Guo A, Salamo G J, Duchesne D, Morandotti R, Volatier-Ravat M, Aimez V, Siviloglou G A and Christodoulides D N 2009 Observation of PT-Symmetry breaking in complex optical potentials

- Phys. Rev. Lett.* **103** 093902
- [47] Rüter C E, Makris K G, El-Ganainy R, Christodoulides D N, Segev M and Kip D 2010 Observation of parity-time symmetry in optics *Nat. Phys.* **6** 192–5
 - [48] Zhu X, Ramezani H, Shi C, Zhu J and Zhang X 2014 PT-symmetric acoustics *Phys. Rev. X* **4** 031042
 - [49] Shi C, Dubois M, Chen Y, Cheng L, Ramezani H, Wang Y and Zhang X 2016 Accessing the exceptional points of parity-time symmetric acoustics *Nat. Commun.* **7** 11110
 - [50] Fleury R, Sounas D L and Alù A 2016 Parity-Time Symmetry in Acoustics: Theory, Devices, and Potential Applications *IEEE J. Sel. Top. Quantum Electron.* **22** 121
 - [51] Yang Y, Jia H, Bi Y, Zhao H and Yang J 2019 Experimental demonstration of an acoustic asymmetric diffraction grating based on Ppassive parity-time-symmetric medium *Phys. Rev. Appl.* **12** 034040
 - [52] Schindler J, Li A, Zheng M C, Ellis F M and Kottos T 2011 Experimental study of active LRC circuits with PT symmetries *Phys. Rev. A* **84** 040101
 - [53] Bittner S, Dietz B, Günther U, Harney H L, Miski-Oglu M, Richter A and Schäfer F 2012 PT Symmetry and spontaneous symmetry breaking in a microwave billiard *Phys. Rev. Lett.* **108** 024101
 - [54] Hang C, Huang G and Konotop V V. 2013 PT Symmetry with a System of Three-Level Atoms *Phys. Rev. Lett.* **110** 083604
 - [55] Bender C M, Berntson B K, Parker D and Samuel E 2013 Observation of PT phase transition in a simple mechanical system *Am. J. Phys.* **81** 173
 - [56] Peng P, Cao W, Shen C, Qu W, Wen J, Jiang L and Xiao Y 2016 Anti-parity-time symmetry with flying atoms *Nat. Phys.* **12** 1139
 - [57] Zhang Z, Zhang Y, Sheng J, Yang L, Miri M-A, Christodoulides D N, He B, Zhang Y and Xiao M 2016 Observation of parity-time symmetry in optically induced atomic lattices *Phys. Rev. Lett.* **117** 123601
 - [58] Fang Y, Kottos T and Thevamaran R 2021 Universal route for the emergence of exceptional points in PT-symmetric metamaterials with unfolding spectral symmetries *New J. Phys.* **23** 063079
 - [59] Fleury R, Sounas D and Alù A 2015 An invisible acoustic sensor based on parity-time symmetry *Nat. Commun.* **6** 5905
 - [60] Wiersig J 2014 Enhancing the sensitivity of frequency and energy splitting detection by using exceptional points: application to microcavity sensors for single-particle detection *Phys. Rev. Lett.* **112** 203901
 - [61] Yu S, Meng Y, Tang J-S, Xu X-Y, Wang Y-T, Yin P, Ke Z-J, Liu W, Li Z-P, Yang Y-Z, Chen G, Han Y-J, Li C-F and Guo G-C 2020 Experimental investigation of quantum PT-enhanced sensor *Phys. Rev. Lett.* **125** 240506
 - [62] Feng L, Xu Y-L, Fegadolli W S, Lu M-H, Oliveira J E B, Almeida V R, Chen Y-F and Scherer A 2013 Experimental demonstration of a unidirectional reflectionless parity-time metamaterial at optical frequencies *Nat. Mater.* **12** 108
 - [63] Jin L, Wang P and Song Z 2017 One-way light transport controlled by synthetic magnetic fluxes and -symmetric resonators *New J. Phys.* **19** 015010
 - [64] Gear J, Sun Y, Xiao S, Zhang L, Fitzgerald R, Rotter S, Chen H and Li J 2017 Unidirectional zero reflection as gauged parity-time symmetry *New J. Phys.* **19** 123041
 - [65] Zhao H, Fegadolli W S, Yu J, Zhang Z, Ge L, Scherer A and Feng L 2016 Metawaveguide for Asymmetric Interferometric Light-Light Switching *Phys. Rev. Lett.* **117** 193901
 - [66] Miri M-A, LiKamWa P and Christodoulides D N 2012 Large area single-mode parity-time-symmetric laser amplifiers *Opt. Lett.* **37** 764
 - [67] Feng L, Wong Z J, Ma R M, Wang Y and Zhang X 2014 Single-mode laser by parity-time symmetry breaking *Science* **346** 972
 - [68] Longhi S and Feng L 2014 PT-symmetric microring laser-absorber *Opt. Lett.* **39** 5026
 - [69] Longhi S 2010 PT-symmetric laser absorber *Phys. Rev. A* **82** 031801

- [70] Chong Y D, Ge L and Stone A D 2011 PT-symmetry breaking and laser-absorber modes in optical scattering systems *Phys. Rev. Lett.* **106** 093902
- [71] Wan W, Chong Y, Ge L, Noh H, Stone A D and Cao H 2011 Time-reversed lasing and interferometric control of absorption *Science* **331** 889
- [72] Robins N P, Figl C, Jeppesen M, Dennis G R and Close J D 2008 A pumped atom laser *Nat. Phys.* **4** 731
- [73] Li J, Harter A K, Liu J, de Melo L, Joglekar Y N and Luo L 2019 Observation of parity-time symmetry breaking transitions in a dissipative Floquet system of ultracold atoms *Nat. Commun.* **10** 855
- [74] Köhl M, Busch T, Mølmer K, Hänsch T W and Esslinger T 2005 Observing the profile of an atom laser beam *Phys. Rev. A* **72** 063618
- [75] Smith D H and Volosniev A G 2019 Engineering momentum profiles of cold-atom beams *Phys. Rev. A* **100** 033604
- [76] Wüster S and El-Ganainy R 2017 Non-Hermitian matter-wave mixing in Bose-Einstein condensates: Dissipation-induced amplification *Phys. Rev. A* **96** 013605
- [77] Raza Sø, Bozhevolnyi S I, Wubs M and Asger Mortensen N 2015 Nonlocal optical response in metallic nanostructures *J. Phys. Condens. Matter* **27** 183204
- [78] Xu D, Xiong X, Wu L, Ren X-F, Png C E, Guo G-C, Gong Q and Xiao Y-F 2018 Quantum plasmonics: new opportunity in fundamental and applied photonics *Adv. Opt. Photonics* **10** 703
- [79] Cerjan A, Xiao M, Yuan L and Fan S 2018 Effects of non-Hermitian perturbations on Weyl Hamiltonians with arbitrary topological charges *Phys. Rev. B* **97** 075128
- [80] Kartashov Y V., Konotop V V. and Zezyulin D A 2014 CPT-symmetric spin-orbit-coupled condensate *Europhysics Lett.* **107** 50002
- [81] Guo S, Dong C, Zhang F, Hu J and Yang Z 2021 Theoretical prediction of non-Hermitian skin effect in ultracold atom systems [arXiv:2111.04220](#)
- [82] Zhou L, Li H, Yi W and Cui X 2021 Engineering non-Hermitian skin effect with band topology in ultracold gases [arXiv:2111.04196](#)
- [83] Sun J Z 2021 Impurity in a Fermi gas under non-Hermitian spin-orbit coupling *Eur. Phys. J. D* **2021** 752 **75** 39
- [84] Watanabe H and Yanase Y 2021 Photocurrent response in parity-time symmetric current-ordered states *Phys. Rev. B* **104** 024416
- [85] Harder M, Yang Y, Yao B M, Yu C H, Rao J W, Gui Y S, Stamps R L and Hu C M 2018 Level Attraction Due to Dissipative Magnon-Photon Coupling *Phys. Rev. Lett.* **121** 137203
- [86] Wu M, Peng R, Liu J, Zhao Q and Zhou J 2020 Energy Band Attraction Effect in Non-Hermitian Systems *Phys. Rev. Lett.* **125** 137703
- [87] Zhou L, Qin J-L, Lan Z, Dong G and Zhang W 2015 Goos-Hänchen shifts in spin-orbit-coupled cold atoms *Phys. Rev. A* **91** 031603
- [88] Qin J, Zheng R and Zhou L 2020 Bound states of spin-orbit coupled cold atoms in a Dirac delta-function potential *J. Phys. B At. Mol. Opt. Phys.* **53** 125301
- [89] Qin J and Zhou L 2020 Unidirectional spin transport of a spin-orbit-coupled atomic matter wave using a moving Dirac δ -potential well *Phys. Rev. A* **102** 013304
- [90] Chen L, Zhang Y and Pu H 2020 Spin squeezing in a spin-orbit-coupled Bose-Einstein condensate *Phys. Rev. A* **102** 023317
- [91] Martone G I, Li Y and Stringari S 2014 Approach for making visible and stable stripes in a spin-orbit-coupled Bose-Einstein superfluid *Phys. Rev. A* **90** 041604
- [92] Martone G I 2015 Visibility and stability of superstripes in a spin-orbit-coupled Bose-Einstein condensate *Eur. Phys. J. Spec. Top.* **224** 553
- [93] Chen X-L, Wang J, Li Y, Liu X-J and Hu H 2018 Quantum depletion and superfluid density of a supersolid in Raman spin-orbit-coupled Bose gases *Phys. Rev. A* **98** 013614
- [94] Makris K G, El-Ganainy R, Christodoulides D N and Musslimani Z H 2008 Beam dynamics in PT Symmetric Optical Lattices *Phys. Rev. Lett.* **100** 103904

- [95] Agrawal G P 2001 *Nonlinear fiber optics* (Academic press: San Diego).